Available online at www.sciencedirect.com

SciVerse ScienceDirect

Ceramics International 39 (2013) 6391–6397

CERAMICS INTERNATIONAL

www.elsevier.com/locate/ceramint

# Multifuctional $Fe_3O_4$@C/$YVO_4$:$Dy^{3+}$ nanopowers: Preparation, luminescence and magnetic properties

Jianhui Shi, Lizhu Tong, Xiaozhen Ren, Quanhong Li, Hua Yang*

*College of Chemistry, Jilin University, Changchun 130012, China*

Received 3 January 2013; received in revised form 6 January 2013; accepted 21 January 2013
Available online 31 January 2013

**Abstract**

As-synthesized $Fe_3O_4$ nanoparticles were encapsulated with carbon layers through a simple hydrothermal process. $Fe_3O_4$/C nanoparticles were coated with $YVO_4$:$Dy^{3+}$ phosphors to form bifunctional $Fe_3O_4$@C@$YVO_4$:$Dy^{3+}$ composites. Their structure, luminescence and magnetic properties were characterized by XRD, SEM, TEM, HRTEM, PL spectra and VSM. The experimental results indicated that the as-prepared bifunctional composites displayed well-defined core–shell structures. The ~12 nm diameter $YVO_4$:$Dy^{3+}$ shell exhibited tetragonal structure. Additionally, the composites exhibited a high saturation magnetization (13 emu/g) and excellent luminescence properties, indicating their promising potential as multifunctional biosensors for biomedical applications.


*Keywords:* B. Composites; C. Magnetic properties; $Fe_3O_4$@C@$YVO_4$: $Dy^{3+}$; Luminescence properties

## 1. Introduction

Complex nanostructures have been attracting much attention because of their multifunction or new applications originating from multicomponent [1–6]. The design and fabrication of multifunctional nanostructures combined with magnetic and fluorescence properties have recently increased interest for biological and biomedical applications. Among them, iron oxides with nanostructures have been extensively studied due to their special magnetic properties. They could be combined with other materials to obtain multifunctional nanocomposites [7,8]. The immobilization of transition metals or their oxides on the magnetic microspheres (MS) could allow them to retain high activity and enable facile separation from the reaction media. However, the combination of different building blocks into an ordered nanostructure is considerably difficult, especially for the components with different crystalline structures. To develop a reliable synthetic method for fabricating multifunctional nanocomposite with designed components and controlled morphologies is still a big challenge.

Recently, surface coated or surface modification nanocomposite has been recognized as one of the most intriguing methods to build complex nanostructures [9,10]. Coating or modification can alter the surface charge and reactivity of the substrate. Compared to polymer and silica shells that have been studied, carbon shells have exhibited much higher stability in various chemical and physical environments such as acid or base media, as well as at high temperatures and pressures. Furthermore, carbon is a special and unique material for coating treatment and core/shell type nanostructures could be thus achieved. Activated –COOH groups could be easily introduced onto the carbon layer by the oxidization treatment [11,12]. As a result, the carboxylic acid functional groups on the carbon layer could give rise to preferred sites of nucleation.

For the fluorescent components, organic fluorophore and quantum dots (QDs) are mostly used [13–15]. Although they have been proven to be quite useful they are still far from perfect because both of them have some inherent limitations. For example, organic fluorophore is prone to photobleaching and has a broad emission and small Stokes shift resulting in cross-talk between excitation and emission signals [16]. QDs are less chemically stable and potentially toxic and may show fluorescence intermittence [17]. Moreover, their inherent

*Corresponding author. Tel.: +86 431 85167712.
*E-mail address:* huayang86@sina.com (H. Yang).

0272-8842/$ - see front matter © 2013 Elsevier Ltd and Techna Group S.r.l. All rights reserved.
http://dx.doi.org/10.1016/j.ceramint.2013.01.065

short-lived luminescence lifetimes may overlap with the spontaneous background emission sources. In comparison with organic dyes and QDs, lanthanide ions related compounds have some unique luminescence properties, such as sharp absorption and emission lines, long lifetimes, superior photostability and effective elimination of short-lived scattering light and background noises [18,19]. Thus they are very favorable for use in bioassays and bio-labeling.

In this article, lanthanide-doped inorganic nanocrystals ($YVO_4$:$Dy^{3+}$) have been chosen as a functional and florescent component for further decoration on the surface of $Fe_3O_4$@C nanoparticles. We report a simple sol–gel process for the preparation of $Fe_3O_4$@C@$YVO_4$:$Dy^{3+}$ composites with excellent magnetic and luminescence properties. Reactive carbon interlayer is introduced in an important role in which it separated lanthanide based luminescent component from the magnetite. The combination of magnetic with luminescent functional groups to form core–shell structured composites is undoubtedly of special interest in enzyme immobilization [20], controlled drug release [21,22], and bioseparation [23] based on their unique magnetic responsivity, visible luminescence, low cytotoxicity, and good biocompatibility.

## 2. Experimental section

### 2.1. Reagents

All reagents are of analytical reagent grade and used without further purification. Ferrous chloride hexahydrate ($FeCl_3 \cdot 6H_2O$; 99%), sodium acetate (NaAc), $Y_2O_3$(99.9%) and $Dy_2O_3$(99.9%) were purchased from Beijing Chemicals Corporation. Citrate acid monohydrate and glucose were purchased from Tianjin chemicals Corporation. Nitric acid ethanol, ethylene glycol (EG) and ammonia aqueous (25%) were purchased from Beijing Chemical Reagents Corporation. Only distilled water was used.

### 2.2. Synthesis of magnetic $Fe_3O_4$ nanoparticles

Magnetic $Fe_3O_4$ nanoparticles were prepared through a modified solvothermal reaction [24]. Typically, 1.35 g of $FeCl_3 \cdot 6H_2O$ and 7.2 g of NaAc were dissolved in 40 mL of ethylene glycol and stirred for 30 min to obtain solution. The solution was transferred into a teflon lined stainless-steel autoclave (50 mL capacity) and heated at 200 °C for 10 h. Then it was cooled to room temperature. The as-synthesized black products were thoroughly washed with ethanol and deionized water three times, and were recovered magnetically.

### 2.3. Synthesis of $Fe_3O_4$@C nanoparticles

$Fe_3O_4$ (0.1 g) powders were ultrasonicated in 0.1 M $HNO_3$ solution for 10 min and washed with deionized water. Then the treated $Fe_3O_4$ microspheres were redispersed in 0.5 M aqueous glucose solution with vigorous stirring for 10 min. The suspension was transferred to autoclaves and maintained at 180 °C for 4 h. The black products ($Fe_3O_4$@C) were separated by magnet and washed with deionized water and ethanol several times, then dried under vacuum at 50 °C for 12 h to obtain $Fe_3O_4$@C nanoparticles.

### 2.4. Synthesis of $Fe_3O_4$@C/$YVO_4$:$Dy^{3+}$ composites

Modification of $YVO_4$:$Dy^{3+}$ on the surface of $Fe_3O_4$@C nanoparticles was achieved according to the reported process with the doping concentration of $Dy^{3+}$ of 1 mol% to $Y^{3+}$ in $YVO_4$:$Dy^{3+}$ [25,26]. The typical procedure for synthesis is described as follows: 0.2231 g (0.99 mmol) of $Y_2O_3$, 0.0037 g (0.01 mmol) of $Dy_2O_3$, and 0.2340 g (2 mmol) of $NH_4VO_3$ were dissolved in dilute $HNO_3$. Then 2.52 g of citric acid (12 mmol) was added as a chelating agent. After stirring for 1 h, a homogeneous gel was formed. Then desired amount of $Fe_3O_4$@C nanoparticles was added into the gel, stirred for 3 h and then dried at 80 °C for 12 h to obtain $Fe_3O_4$@C/$YVO_4$:$Dy^{3+}$ composites.

### 2.5. Characterization

The morphology of all the as-synthesized samples was characterized by a scanning electronic microscope (SEM; Philips XL-30). The transmission electron microscopy (TEM) and high resolution transmission electron microscopy (HRTEM) images were obtained on a field-emission transmission electron microscope (TECNAI G2; 200 kV). The structural properties of all the samples were checked by X-ray diffraction measurements at room temperature using Cu-K$\alpha$ radiation (K$\alpha$ = 1.54059 Å). Magnetic properties of samples were measured by a vibration sample magnetometer at room temperature. A spectrophotometer (Hitachi F-4500 spectrophotometer equipped with a 150 W xenon lamp as the excitation source) was used for the photoluminescence (PL) measurement at room temperature.

## 3. Results and discussion

We have successfully synthesized bifunctional $Fe_3O_4$@C/$YVO_4$:$Dy^{3+}$ composites with magnetic and luminescence properties. The formation process of the composites is shown in Fig. 1. The $Fe_3O_4$ magnetite particles were synthesized by the solvothermal method with $FeCl_3$ as the iron source and ethylene glycol as both solvent and reductant [27]. Herein, in the preparation process, the $Fe_3O_4$ nanoparticles are successfully modified with a thin carbon layer after hydrothermal reaction with the glucose. A carbon layer coated on the surface of magnetite particles is of great interest to enhance their dispensability in aqueous solution and prevents them from aggregating in liquid media. In addition, the carbon layer as a shell can protect the $Fe_3O_4$. Furthermore, the carboxyl groups can be endowed to $Fe_3O_4$@C nanoparticles with excellent affinity between the $Fe_3O_4$@C nanoparticles

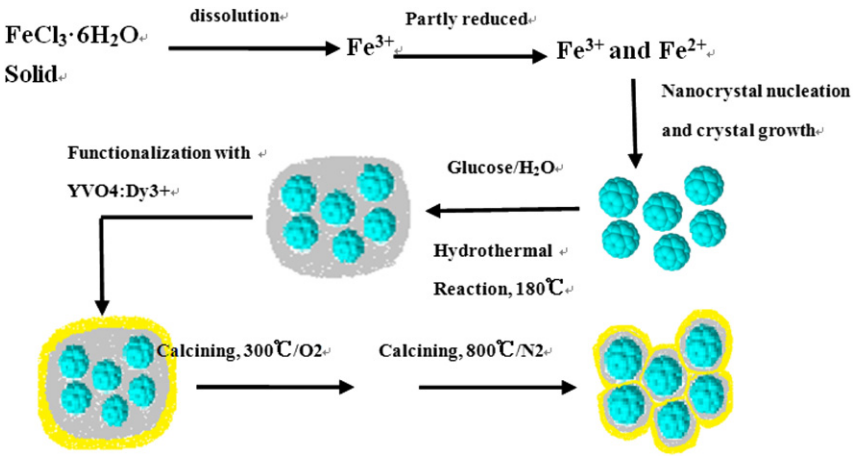


Fig. 1. Schematic illustration of the preparation of $Fe_3O_4$@C/$YVO_4$:$Dy^{3+}$ composites.

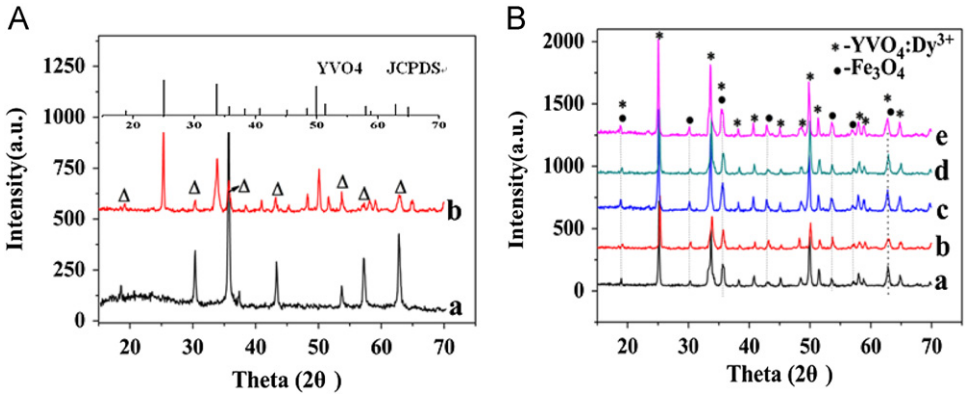


Fig. 2. XRD patterns of $Fe_3O_4$@C (A-a), $Fe_3O_4$@C/$YVO_4$:$Dy^{3+}$ (A-b) and $Fe_3O_4$@C@/$YVO_4$:$Dy^{3+}$ (B) with different doped concentrations of $Dy^{3+}$ ions (a: 0.5%, b: 1%, c: 2%, d: 3% and e: 4%).

and modified species. Thus easily, $YVO_4$:$Dy^{3+}$ precursor is deposited on the surface of $Fe_3O_4$@C nanoparticles by the sol–gel method. Finally, the $Fe_3O_4$@C/$YVO_4$:$Sm^{3+}$ composites are preheated at 300 °C exposed to the air, after which, the samples continued to be calcined at 800 °C under condition of $N_2$ atmosphere.

Fig. 2A shows XRD patterns of $Fe_3O_4$@C nanoparticles and $Fe_3O_4$@C/$YVO_4$:$Dy^{3+}$ composites. The XRD diffraction peaks located at $2\theta = 30.1°$, 35.8°, 43.1°, 53.8°, 57.3° and 63.0° can be indexed to (220), (311), (400), (422), (511), and (440) planes of $Fe_3O_4$ in a face-centered cubic (fcc) $Fe_3O_4$ (JCPDS card no. 19-629), respectively. The broadened peak centered at a small angle ($2\theta < 30°$) indicated the presence of amorphous carbon shells, which is pointed with a black arrow in Fig. 2A(a). Compared with XRD patterns of the $Fe_3O_4$@C and the JCPDS of $YVO_4$:$Dy^{3+}$, besides the characteristic diffractions of cubic $Fe_3O_4$, the obvious diffraction peaks of $Fe_3O_4$@C/$YVO_4$:$Dy^{3+}$ can be indexed to the tetragonal phase of $YVO_4$ (JCPDS no.17-0341), suggesting the successful crystallization of $YVO_4$:$Dy^{3+}$ on the surface of magnetite core. Moreover, no additional peaks for other phases are detected, indicating that pure $Fe_3O_4$@C/$YVO_4$:$Dy^{3+}$ composites are prepared. Additionally, Fig. 2B gives the XRD patterns of $Fe_3O_4$@C@/$YVO_4$:$Dy^{3+}$ with different doped concentrations of $Dy^{3+}$ ions, which indicated that the $Dy^{3+}$ doped concentration has not changed the structure of $Fe_3O_4$@C@/$YVO_4$:$Dy^{3+}$ composites. However, it has important influences on the PL properties of composites, and this point will be studied in the later part of the article.

SEM images of $Fe_3O_4$, $Fe_3O_4$@C and $Fe_3O_4$@C/$YVO_4$:$Dy^{3+}$ are shown in Fig. 3. From Fig. 3A, we can observe that $Fe_3O_4$ nanoparticles are monodispersed and have rough surface. Additionally, the nanoparticles are non-aggregated and have narrow particle size distribution. Fig. 3B shows that the $Fe_3O_4$@C nanoparticles are still spheres and their diameter is about 200 nm. Interestingly, the surface of the $Fe_3O_4$@C nanoparticles is much smoother than that of pure $Fe_3O_4$, further indicating the uniform carbon shell coated on the $Fe_3O_4$. As for $Fe_3O_4$@C/$YVO_4$:$Dy^{3+}$ composites (Fig. 3C), the morphological features are very similar to $Fe_3O_4$@C, such as the spherical morphology and smooth surface. Furthermore, no irregular particles related with the introduced phosphors are detected. The results suggested that the deposition had a little influence on the spherical morphology and the phosphor layers are uniformly dispersed on the surface of $Fe_3O_4$@C nanoparticles.

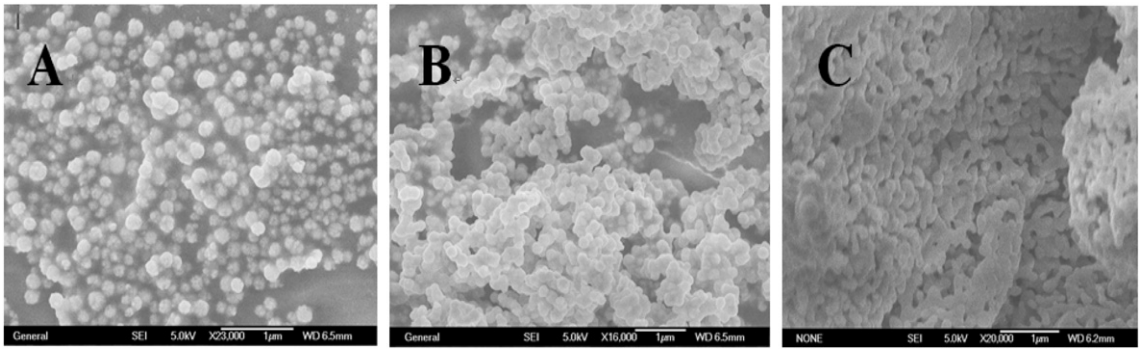


Fig. 3. SEM images of $Fe_3O_4$ (A), $Fe_3O_4$@C (B) and $Fe_3O_4$@C/$YVO_4$:$Dy^{3+}$ composites (C).

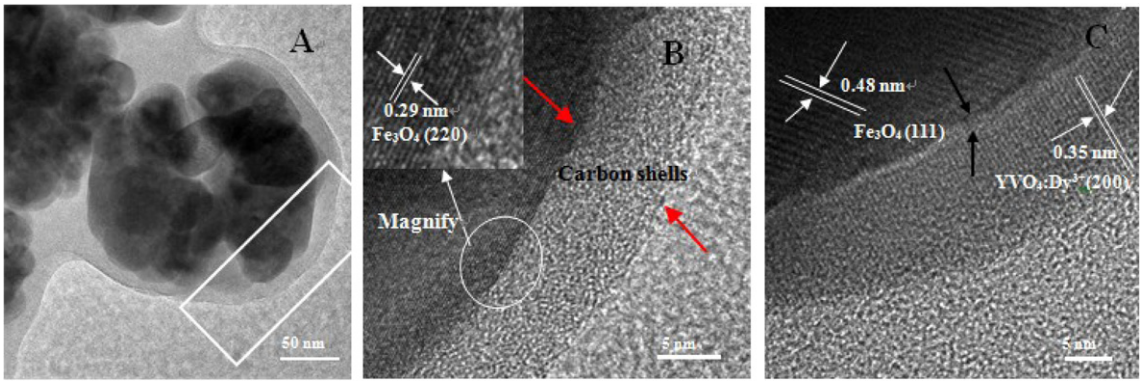


Fig. 4. TEM image of $Fe_3O_4$@C (A), HRTEM images of the marked square region of A (B) and $Fe_3O_4$@C/$YVO_4$:$Dy^{3+}$ (C).

The morphological and structural features of the samples were further examined by TEM and HRTEM in Fig. 4. From Fig. 4A, it is shown that the $Fe_3O_4$@C nanoparticles are spheres and have core–shell structure. Their particle sizes are about ~200 nm, and thickness of the carbon layer is about ~10 nm. The uniform amorphous carbon is formed by the carbonization of glucoses on the surface of the $Fe_3O_4$ particles involving intermolecular cross-linking and dehydration of the glucoses, oligosaccharides, and/or other macromolecules derived from glucose during the hydrothermal treatment [28]. Moreover, from HRTEM image of Fig.4B, it is shown that carbon layer as a shell is on the surface of $Fe_3O_4$ and amorphous, and the d spacing of core is 0.29 nm and indexed to the (220) crystal plane of the $Fe_3O_4$ nanoparticles. Additionally, the HRTEM image of $Fe_3O_4$@C/$YVO_4$:$Dy^{3+}$ (Fig. 4C) shows high crystallinity and is in good agreement with the XRD results (Fig. 2). The distance of 0.35 nm between the adjacent lattice fringes is in agreement with the $d_{200}$ spacing (200) of the tetragonal $YVO_4$ phase. And the d spacing of the core is 0.48 nm; it is indexed to the (111) crystal plane of the $Fe_3O_4$ nanoparticles. Notably, the interface between $Fe_3O_4$ and $YVO_4$:$Dy^{3+}$ is carbon layer, and thickness of the carbon layer is about 2 nm, which may separate lanthanide based luminescent component from the $Fe_3O_4$ magnetite and decrease the quenching effect resulting from the $Fe_3O_4$ magnetite.

The magnetic properties of $Fe_3O_4$@C/$YVO_4$:$Dy^{3+}$ composites were characterized by a vibrating sample magnetometer at room temperature in Fig. 5A. As shown by the magnetic hysteresis loops, the composites exhibit typical ferromagnetic curves. The saturation magnetization $M_s$ values of the $Fe_3O_4$ nanoparticles, $Fe_3O_4$@C microspheres and $Fe_3O_4$@C/$YVO_4$:$Dy^{3+}$ composites are 80, 60 and 13 emu/g, respectively. The $M_s$ of $Fe_3O_4$@C/$YVO_4$:$Dy^{3+}$ composites is the lowest, which may be due to the amorphous carbon interfaces and the presence of the nonmagnetic phosphor providing less magnetic moment per unit mass than that of ferromagnetic core [29]. At the same time, Fig. 5(B) shows the magnetic hysteresis loops of $Fe_3O_4$@C/$YVO_4$:$Dy^{3+}$ composites with a different molar ratio of the core and the shell, and it is clear that the composites have lower $M_s$ with the increase of content of phosphor shells. Additionally, we can observe that all the composites with different ratios have remanence ($B_r$) and coercive force ($H_c$). The possible reason is that compared with the pure $Fe_3O_4$, there are some impurities in the composites, such as lattice defects, hole and different phase, which make the lattice magnetic domains bigger and lead to increase of remanence. Of course, the coercive force also becomes bigger.

The luminescence properties of the samples were further characterized by the excitation and the emission spectra, as shown in Figs. 6–8. Fig. 6 shows the excitation spectra and emission spectra of $Fe_3O_4$@C/$YVO_4$:$Dy^{3+}$ composites

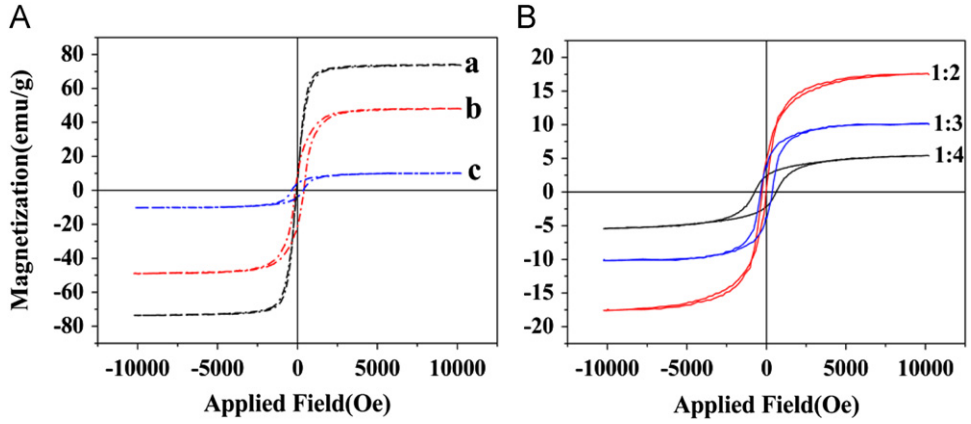


Fig. 5. (A) The magnetic hysteresis loops of pure $Fe_3O_4$ (A-a), $Fe_3O_4$@C (A-b), $Fe_3O_4$@C/$YVO_4$:$Dy^{3+}$ (A-c) and $Fe_3O_4$@C/$YVO_4$:$Dy^{3+}$ (B) with different molar ratios of core and shell.

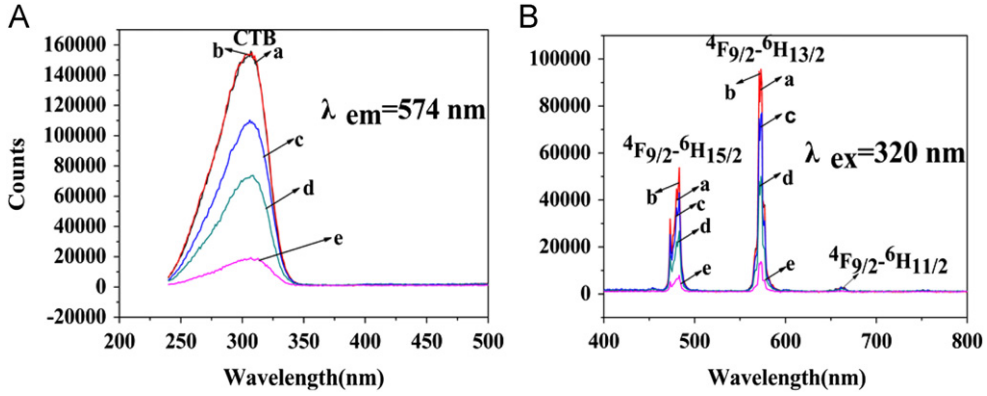


Fig. 6. Excitation spectra (A) and emission spectra (B) of $Fe_3O_4$@C/$YVO_4$:$Dy^{3+}$ with different doped concentrations of $Dy^{3+}$ (a: 0.5%, b: 1%, c: 2%, d: 3% and e: 4%).

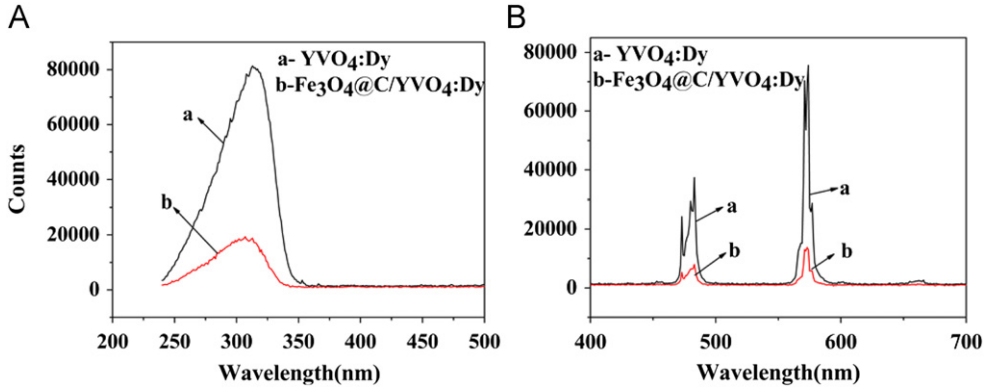


Fig. 7. Excitation spectra (A) and emission spectra (B) of $YVO_4$:$Dy^{3+}$ (a) and $Fe_3O_4$@C/$YVO_4$:$Dy^{3+}$ (b) composites.

with different doped concentration of $Dy^{3+}$ ions. It is shown that the optimum doped concentration of $Dy^{3+}$ ions in the $Fe_3O_4$@C/$YVO_4$:$Dy^{3+}$ composites is 1%. Additionally, the luminescence intensities are decreased with increasing doped concentration of $Dy^{3+}$. In the excitation spectra in Fig. 6A, the strong excitation band of the composites is at about 325 nm at the emission wavelength of 574 nm, which is ascribed to a charge transfer from the oxygen ligands to the central vanadium atom inside the $VO_4^{3-}$ group ions. In the emission spectra of the composites (Fig. 6B), it is shown that the electronic transition lines of $Dy^{3+}$ from $^4F_{9/2}$–$^6H_{13/2}$ to $^4F_{9/2}$ –$^6H_{15/2}$ are observed and $^4F_{9/2}$–$^6H_{13/2}$ hypersensitive electronic transition ($\Delta J=2$) dominates. It is because the $Dy^{3+}$ ions

in the $YVO_4$ host lattices are located at a low symmetry local site $D_{2d}$ without inversion center in the $YVO_4$ host lattices [30]. Moreover, the presence of the $VO_4^{3-}$ absorption in the excitation spectra of $Dy^{3+}$, indicates that an energy transfer occurs in the electronic transition from $VO_4^{3-}$ ions to $Dy^{3+}$ ions in $YVO_4$:$Dy^{3+}$, and the energy transfer is very efficient because the emission of $VO_4^{3-}$ is not observed and only the emission of $Dy^{3+}$ is observed upon excitation at $VO_4^{3-}$. The energy transferring from $VO_4^{3-}$ to $Dy^{3+}$ is dominated by exchange interaction at room temperature like energy transfer between $VO_4^{3-}$ and $Dy^{3+}$ ions in $YVO_4$ [25]. Fig. 7 gives the excitation spectra and emission spectra of $YVO_4$:$Dy^{3+}$ and $Fe_3O_4$@C/$YVO_4$:$Dy^{3+}$ composites. For the $Fe_3O_4$@C/$YVO_4$:$Dy^{3+}$ composites, it is clear that both the intensities of excitation spectra and emission spectra decrease. It is because the quenching effect for $YVO_4$:$Dy^{3+}$ resulted from $Fe_3O_4$. Fortunately, the $Fe_3O_4$@C/$YVO_4$: $Dy^{3+}$ composites still show a clear yellow–green light under the UV-light. Fig. 8 shows the excitation spectra and emission spectra of the composites with different mass ratios of core and shell. It is clear that the intensities in both the excitation spectra and emission spectra bands are stronger with decrease in the mass ratio of core and shell. Unfortunately, the relative strong luminescence is always accompanied with the weak magnetism. When the mass ratio is 1:3, there are excellent luminescence and magnetic properties of $Fe_3O_4$@C/$YVO_4$:$Dy^{3+}$.

Fig. 9 gives the magnetic separation photograph of $Fe_3O_4$@C/$YVO_4$:$Dy^{3+}$ dispersed in ethanol under UV excitation at 323 nm and without UV-light. We can see that the $Fe_3O_4$@C/$YVO_4$:$Dy^{3+}$ composites disperse well in ethanol, and emit obvious yellow–green luminescence. When we put a magnet near the squart cell, the nanocomposites accumulate near the magnet and still emit yellow–green light. These photographs can prove that we have successfully synthesized bifunctional magnetic–optical nanoparticles. And the results are in agreement with the above PL and magnetic results, which endow the $Fe_3O_4$@C/$YVO_4$:$Dy^{3+}$ composites with potential application in biological fields, such as biosensors for simultaneous labeling, sorting and separation of cancer cells.

## 4. Conclusion

In conclusion, we report the synthesis of a novel magnetic/luminescence bifunctional composite $Fe_3O_4$@C/$YVO_4$:$Dy^{3+}$ with core–shell structure by a combination of hydrothermal reaction and the sol–gel process. The as-obtained $Fe_3O_4$@C/$YVO_4$:$Dy^{3+}$ microspheres have a mean diameter of ~200 nm and uniform $YVO_4$:$Dy^{3+}$ shell (about 10 nm in thickness). Furthermore, the carbon layers of ~2 nm still remain in the composites, which may separate lanthanide based luminescent component from

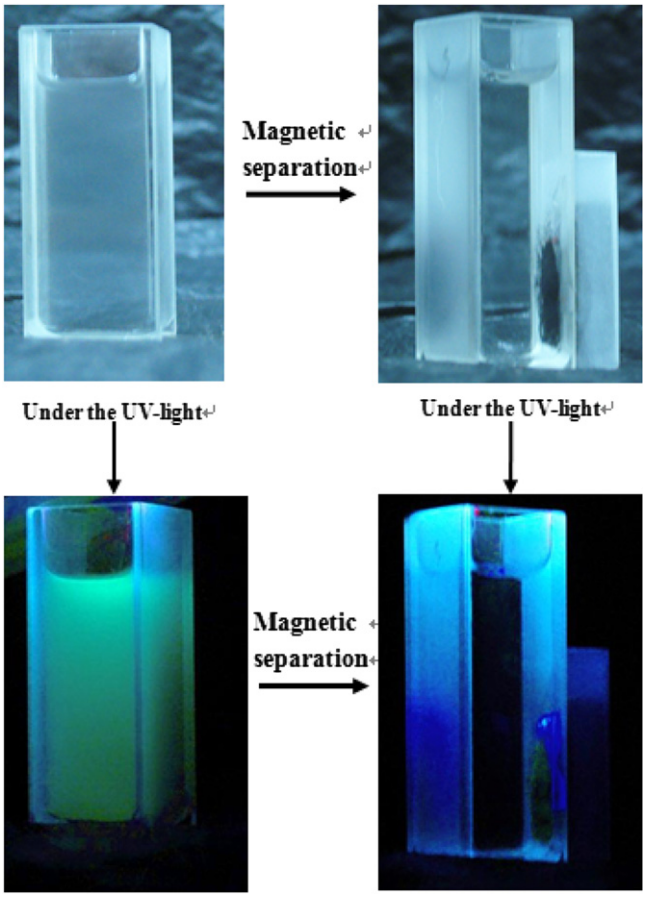


Fig. 9. The magnetic separation photograph of $Fe_3O_4$@C/$YVO_4$:$Dy^{3+}$.

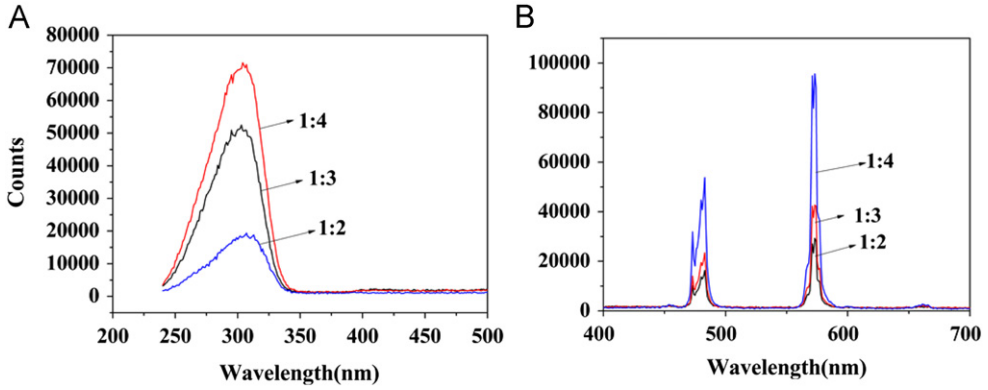


Fig. 8. Excitation spectra (A) and emission spectra (B) of $Fe_3O_4$@C/$YVO_4$:$Dy^{3+}$ with different molar ratios of core and shell.

the magnetite to decrease the fluorescent quenching effect resulting from the $Fe_3O_4$ magnetite. More importantly, the as-prepared bifunctional composites combined the advantages of magnetism and luminescence, which make the composites have a potential application in more biological fields.

## Acknowledgments

This work was supported by the National Natural Science Foundation of China.

## References

[1] J.H. Park, L. Gu, G. von Maltzahn, E. Ruoslahti, S.N. Bhatia, M.J. Sailor, Biodegradable luminescent porous silicon nanoparticles for in vivo applications, Nature Materials 8 (2009) 331–336.
[2] Q. Sun, Q. Wang, P. Jena, Y. Kawazoe, Design of Janus nanoparticles with atomic precision: tungsten-doped gold nanostructures, ACS Nano 2 (2008) 341–347.
[3] V. Sharma, J. Jiang, M. Hossu, A.R. Koymen, S. Priya, Self-assembled periodic nanoporous network in multifunctional $ZrO_2$–$CeO_2$–($La_{0.8}Sr_{0.2}$) $MnO_3$ composites, Applied Physics Letters 90 (2007) 123110-1–123110-3.
[4] C.L. Lo, K.M. Lin, C.K. Huang, G.H. Hsiue, Self-assembly of a Micelle structure from Graft and Diblock copolymers: an example of overcoming the limitations of polyions in drug delivery, Advanced Functional Materials 16 (2006) 2309–2316.
[5] M. Chen, Y.N. Kim, H.M. Lee, C. Li, S.O. Cho, Multifunctional magnetic silver nanoshells with sandwich-like nanostructures, The Journal of Physical Chemistry C 112 (2008) 8870–8874.
[6] M. Chen, Y.N. Kim, C. Li, S.O. Cho, Preparation and characterization of magnetic nanoparticles and their silica egg-yolk-like nanostructures: a prospective multifunctional nanostructure platform, The Journal of Physical Chemistry C 112 (2008) 6710–6716.
[7] J.P. Fortin, C. Wilhelm, J. Servais, C. Menager, J.C. Bacri, F. Gazeau, Size-sorted anionic iron oxide nanomagnets as colloidal mediators for magnetic hyperthermia, Journal of the American Chemical Society 129 (2007) 2628–2635.
[8] U. Jeong, X.W. Teng, Y. Wang, H. Yang, Y.N. Xia. Superparamagnetic colloids: controlled synthesis and niche applications. Advanced Materials 19 (2007) 33–60.
[9] F. Caruso, Nanoengineering of particle surfaces, Advanced Materials 13 (2001) 11–22.
[10] R.A. Caruso, M. Antonietti, Sol–gel nanocoating: an approach to the preparation of structured materials, Chemistry of Materials 13 (2001) 3272–3282.
[11] J. Zhang, H.L. Zou, Q. Qing, Y.L. Yang, Q.W. Li, Z.F. Liu, X.Y. Guo, Z.L. Du, Effect of chemical oxidation on the structure of single-walled carbon nanotubes, The Journal of Physical Chemistry B 107 (2003) 3712–3718.
[12] D.B. Mawhinney, V. Naumenko, A. Kuznetsova, J.T. Yates, J. Liu, R.E. Smalley, Infrared spectral evidence for the etching of carbon nanotubes: ozone oxidation at 298 K, Journal of the American Chemical Society 122 (2000) 2383–2384.
[13] C.W. Lu, Y. Hung, J.K. Hsiao, et al., Bifunctional magnetic silica nanoparticles for highly efficient human stem cell labeling, Nano Letters 7 (2007) 149–154.
[14] D.K. Yi, S.T. Selvan, S.S. Lee, et al., Silica-coated nanocomposites of magnetic nanoparticles and quantum dots, Journal of the American Chemical Society 127 (2005) 4990–4991.
[15] J.H. Lee, Y.W. Jun, S.I. Yeon, et al., Dual-mode nanoparticle probes for high-performance magnetic resonance and fluorescence imaging of neuroblastoma, Angewandte Chemie International Edition 45 (2006) 8160–8162.
[16] Z.Q. Ye, M.Q. Tan, G.L. Wang, et al., Novel fluorescent europium chelate-doped silica nanoparticles: preparation, characterization and time-resolved fluorometric application, Journal of Materials Chemistry 14 (2004) 851–856.
[17] I.L. Medintz, H.T. Uyeda, E.R. Goldman, et al., Quantum dot bioconjugates for imaging, labelling and sensing, Nature Materials 4 (2005) 435–446.
[18] T. Steinkamp, U. Karst, Detection strategies for bioassays based on luminescent lanthanide complexes and signal amplification, Analytical and Bioanlaytical Chemistry 380 (2004) 24–30.
[19] M. Nichkova, D. Dosev, S.J. Gee, et al., Microarray immunoassay for phenoxybenzoic acid using polymer encapsulated Eu:$Gd_2O_3$ nanoparticles as fluorescent labels, Analytical Chemistry 77 (2005) 6864–6873.
[20] X.Q. Xu, C.H. Deng, M.X. Gao, W.J. Yu, P.Y. Yang, X.M. Zhang, Synthesis of magnetic microspheres with immobilized metal ions for enrichment and direct determination of phosphopeptides by matrix-assisted laser desorption ionization mass spectrometry, Advanced Materials 18 (2006) 3289–3293.
[21] P.P Yang, Z.W Quan, L.L Lu, S.S Huang, J Lin., A magnetic, luminescent and mesoporous core–shell structured composite material as drug carrier, Biomaterials 29 (2008) 4341–4347.
[22] M Arruebo, C Marquina, MR Ibarra, et al., Development of magnetic nanostructured silica-based materials as potential vectors for drug-delivery applications, Chemistry of Materials 18 (2006) 1911–1919.
[23] Y Li, B Yan, C.H Deng, W.J Yu, X.Q Xu, P.Y Yang, et al., Efficient on-chip proteolysis system based on functionalized magnetic silica microspheres, Proteomics 7 (2007) 2330–2339.
[24] X.Q. Xu, C.H. Deng, M.X. Gao, W.J. Yu, P.Y. Yang, X.M. Zhang, Synthesis of magnetic microspheres with immobilized metal ions for enrichment and direct determination of phosphopeptides by matrix-assisted laser desorption ionization mass spectrometry, Advanced Materials 18 (2006) 3289–3293.
[25] B Amurisana, H. Yang, C. Tao, Y. Zhang, L.l. Han, Luminescent properties of nanoparticles $YP_xV_{1-x}O_4$:Dy phosphors, Journal of Luminescence 128 (2008) 60–66.
[26] E. Cavalli, M. Bettinelli, A. Belletti, A. Speghini, Optical spectra of yttrium phosphate and yttrium vanadate single crystals activated with $Dy^{3+}$, Journal of Alloys and Compounds 341 (2002) 107–110.
[27] H. Deng, X. Li, Y. Li, Q Peng, S. Wang, J. Chen, Y. Li., Monodisperse magnetic single-crystal ferrite microspheres, Angewandte Chemie International Edition 44 (2005) 2782–2785.
[28] X. Sun, Y. Li, Colloidal carbon spheres and their core/shell structures with noble-metal nanoparticles, Angewandte Chemie International Edition 43 (2004) 597–601.
[29] K Tamura, H. Endo, Ferromagnetic properties of amorphous nickel, Physics Letters 29 (1969) 52–53.
[30] J.M. Nedelec, D. Avignant, R. Mahiou, Soft chemistry routes to $YPO_4$-based phosphors: dependence of textural and optical properties on synthesis pathways, Chemistry of Materials 14 (2002) 651–655.